

RD-A179 720

EXPERIMENTAL AND NUMERICAL INVESTIGATION OF COHERENT
STRUCTURES IN TURBUL. (U) ARIZONA UNIV TUCSON
ENGINEERING EXPERIMENT STATION F M CHAMPAGNE ET AL.

1/1

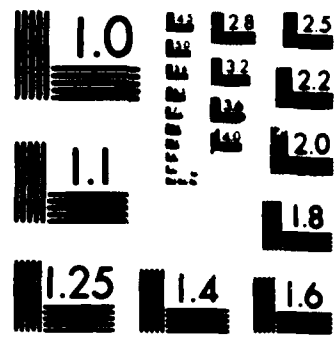
UNCLASSIFIED

07 APR 87 AFOSR-TR-87-0544 AFOSR-85-0146

F/G 1/1

NL





MICROCOPY RESOLUTION TEST CHART
NATIONAL BUREAU OF STANDARDS 1963-A

DTIC FILE COPY

2

SECU

AD-A179 720

DTIC DOCUMENTATION PAGE

1a. REPORT SECURITY CLASSIFICATION UNCLASSIFIED		1b. RESTRICTIVE MARKINGS	
2a. SECURITY CLASSIFICATION AUTHORITY SELECTED		3. DISTRIBUTION/AVAILABILITY OF REPORT	
2b. DECLASSIFICATION/DOWNGRADING SCHEDULE 1987		Approved for public release, distribution unlimited	
4. PERFORMING ORGANIZATION REPORT NUMBER(S) D		5. MONITORING ORGANIZATION REPORT NUMBER(S) AFOSR-TM 87-0544	
6a. NAME OF PERFORMING ORGANIZATION University of Arizona	6b. OFFICE SYMBOL (if applicable) N/A	7a. NAME OF MONITORING ORGANIZATION Air Force Office of Scientific Research	
6c. ADDRESS (City, State and ZIP Code) Engineering Experiment Station College of Engineering and Mines Tucson, Arizona 85721		7b. ADDRESS (City, State and ZIP Code) Bolling Air Force Base Building 410 Washington, D. C. 20332	
8a. NAME OF FUNDING/SPONSORING ORGANIZATION Air Force Office of Scientific Research	8b. OFFICE SYMBOL (if applicable) AFOSR/NR	9. PROCUREMENT INSTRUMENT IDENTIFICATION NUMBER AFOSR 85-0146	
10. SOURCE OF FUNDING NOS.			
PROGRAM ELEMENT NO.	PROJECT NO.	TASK NO.	WORK UNIT NO.
11. TITLE (Include Security Classification) Numerical Investigation of Coherent Structures in Turbulent Wake Flows		61102-F 2307 A2	
12. PERSONAL AUTHOR(S) F. H. Champagne and H. Fasel			
13a. TYPE OF REPORT Annual	13b. TIME COVERED FROM <u>2/5/86</u> TO <u>2/4/87</u>	14. DATE OF REPORT (Yr., Mo., Day) <u>4/7/87</u>	15. PAGE COUNT <u>18</u>
16. SUPPLEMENTARY NOTATION			
17. CCSATI CODES		18. SUBJECT TERMS (Continue on reverse if necessary and identify by block number) <i>Turbulence, Turbulent wakes,</i>	
FIELD	GROUP	SUB. GR.	
19. ABSTRACT (Continue on reverse if necessary and identify by block number) Recent x-wire measurements in a plane turbulent wake are presented. Sinuous disturbances at several amplitudes and frequencies were introduced to the wake by oscillating a small trailing edge flap. The Strouhal numbers of the perturbations were specially chosen so that the downstream location of the neutral point (where the spatial amplification rate obtained from linear stability theory vanishes) was well within the range of measurements. The streamwise variation of the half width of the wake and the centerline velocity deficit was dependent on the amplitude level and showed dramatic deviations at large forcing levels from the well-known square root behavior of the unforced case. The measured coherent Reynolds stresses were observed to change sign in the neighborhood of the location of the neutral point as predicted by linear viscous theory. The numerical simulations of free shear layers and progress towards the wake simulations are also discussed.			
20. DISTRIBUTION/AVAILABILITY OF ABSTRACT UNCLASSIFIED/UNLIMITED <input checked="" type="checkbox"/> SAME AS RPT. <input type="checkbox"/> DTIC USERS <input type="checkbox"/>		21. ABSTRACT SECURITY CLASSIFICATION UNCLASSIFIED	
22a. NAME OF RESPONSIBLE INDIVIDUAL Dr. J. M. McMichael		22b. TELEPHONE NUMBER (Include Area Code) (202) 767-9987	22c. OFFICE SYMBOL AFOSR/NR

AIR FORCE OFFICE OF SCIENTIFIC RESEARCH (AFSC)

NOTE OF TRANSMITTAL TO DTIC

This technical report has been reviewed and is
allowed for public release IAW AFR 190-12.
Distribution is unlimited.

MATTHEW J. KERPER

Chief, Technical Information Division

DTIC FILE COPY

AFOSR-TR- 87-0544

ANNUAL REPORT

AFOSR Contract No. 85-00146

Approved for public release;
distribution unlimited.

Experimental

A considerable amount of new data, including x-wire measurements, has been obtained in the turbulent wake behind a flat plate. Sinuous disturbances at several amplitudes and frequencies were introduced into the wake by oscillating a small trailing edge flap. The Strouhal numbers of the perturbations were specially chosen so that the down stream location of the neutral point (where the spatial amplification rate obtained from linear stability theory vanishes) was well within the range of measurements. The streamwise variation of the half width of the wake, L_0 , and the centerline velocity deficit, u_0 , were dependent on the amplitude level for a fixed frequency. Large deviations from the well known square root behavior are observed at large amplitude forcing levels starting in the region of the neutral point. This is shown in Figure 1 where $L_0 U_\infty / u_0 \theta$, a nondimensional growth variable is plotted versus $(x-x_0)/\theta$ for a forcing frequency, f , of 70 hz and several forcing amplitudes. U_∞ is the free stream velocity, θ is the momentum thickness, and x_0 is the virtual origin. θ remains effectively constant for these cases. The unforced case shows linear behavior as the ratio of L_0/u_0 is proportional to x , the downstream coordinate. The rate of growth for the forced cases is initially larger than that for the unforced case. Depending on the level of forcing, however, the wake stops growing at some downstream location and

appears to be in a state of nearly parallel flow. In the high amplitude case the wake even contracted some and then resumed growing at a slower rate. The downstream location where the wake stops growing in each case roughly corresponds to the location of the neutral point for that case. The exact location of the neutral point is difficult to determine as non-linear terms are not negligible near the end of the amplified region. The variation in the growth rate of the wake near the neutral point is caused by the nonlinear interaction of the perturbation wave with the mean flow. In the region upstream of the neutral point, the disturbances are being amplified and energy is transferred from the mean flow to the disturbance. The wave induced stress changes sign through the neutral point, so downstream of the neutral point energy is transferred from the disturbance to the mean flow. This demonstrates that the lateral rate of spread of the wake is closely linked with the growth of the disturbance wave; amplification of the wave results in a transfer of energy from the mean flow and a divergence of the mean flow. Further evidence to substantiate this can be obtained from noting that the initial divergence of the wake increases with increasing forcing amplitude. The contraction of the wake may be attributed to the transfer of energy from the disturbance wave to the mean flow in the damped region beyond the neutral point.

To consider some of the interesting features of the downstream development of a sinuous wave, let's examine the case of a medium amplitude 80 hz wave. Figure 2 shows the nondimensional growth variable $L_0 U_\infty / u_0 \theta$ versus $(x-x_0)/2^\theta$. The measured mean velocity profiles for various downstream locations are presented in Figure 3 in self preserving form.

/ Codes

INSPECTED 2	Dist	Avail and/or Special
A-1		

Figure 3a shows the profiles for the downstream region labelled a. These profiles agree well with those for the unforced case shown by the solid curve, which represents a curve fit to the unforced profiles. The profiles for the region b, located just past the neutral point, differ from the unforced data as shown in Figure 3b. Further downstream in region c, the changes are more significant. The three regions defined in Figure 3 correspond to the amplified, neutral and damped regions respectively in the context of linear stability theory.

Solution to the inviscid Orr-Summerfeld equation using the appropriate measured mean velocity profile gives the eigenfunction distributions typical for each region. In Figure 4 these solutions are presented in the form of the amplitude and phase of the u component of the disturbance wave. Note the dramatic change in the phase of the u component in the damped region. The phase of the v component does not change sign, and therefore the sign of the wave induced or coherent Reynolds stress changes in the neutral region. The computed wave induced or coherent stress distributions are shown in Figure 5. Four plots are presented for the neutral region showing the downstream evolution of the change in sign. In Figure 6, typical measured amplitude and phase distributions of the u component for each region are presented for comparison. The measured coherent, turbulent and total Reynolds stress for the three regions are displayed in Figure 7. The vertical markers above the data presented in Figure 2 indicate the measurement locations for the data shown. Three data sets are shown for the neutral region demonstrating the change in sign of the coherent stress. Each distribution has been normalized by the maximum value of the total

stress corresponding to that downstream location, so the relative amount of coherent and turbulent stress can be determined. Figure 7a shows the measured stresses in the amplified region. Notice the sign of the coherent stress is the same as that of the turbulent stress, while its magnitude is roughly twice that of the turbulent stress. In Figure 7e, the measured stresses in the damped region c are presented. Note that sign of the coherent stress has changed and its magnitude is now only one-third of that of the turbulent stress.

Figure 8 presents the downstream development of the integral amplitudes of u^2 , v^2 , and uv in the wave component at the fundamental frequency. Each variable is decomposed into its coherent (phase averaged) and turbulent parts and non-dimensionalized by u_0 and L_0 . The peak in the v component of the fundamental occurs at about the downstream location of the neutral point and corresponds to the position where the growth rate of the wake changes as can be seen from Figure 2. Both u and uv peak sooner than v , for both the fundamental and harmonic. Note that at large x , the coherent stress is vanishing while the turbulent part is increasing and approaching a value which is characteristic of the self preserving unforced wake. A comparison of the evolution of the fundamental and harmonic for v is shown in Figure 9. As is readily apparent, the harmonic is more than an order of magnitude smaller. The measured amplitude and phase distributions of the U component of the harmonic are shown in Figure 10.

Numerical Simulations

In the past year, we made considerable progress towards development of a numerical method that will be applicable for investigations of the dynamics of coherent structures in turbulent wakes. As mentioned in last year's report for the actual development of the numerical methods for solving the complete Navier-Stokes equations, we decided to use a different, but related, flow geometry, namely that of a free shear layer. The main motivation for this was the fact that for free shear layers a considerably larger body of substantiated experimental results are available than for wake flows. Therefore, a thorough check of our new numerical methods is possible before applying it to investigations of wake flows. The development of a numerical method which was based on a "temporal" approach (disturbances simplify or decay in time) was already concluded some time ago, and we reported it in last year's report. During the past year, we concluded the development of a numerical method for solving the complete Navier-Stokes equations which is based on the "spatial" approach. (Ph.D. Thesis by C. D. Pruett) The method enables realistic simulations of linear and nonlinear development of stability waves where development (growth or decay) of the disturbances is spatial (in downstream and/or spanwise direction) as in real laboratory experimental situations. In particular, since the nonlinear effects are fully incorporated, it allows us to investigate the saturation of the instability waves, and therefore the intensity of the coherent structures can be predicted. In addition, due to the three-dimensional capability, we

can also investigate the importance of three-dimensional effects or study the breakdown of two-dimensional structures into three-dimensional ones.

Typical results obtained from simulations of a transitional shear layer as shown in Figure 11 and Figure 12). Figure 11 shows the downstream growth of various wave components for a forced transitional free shear layer. Comparison with experiments by Miksad (1972) shows excellent qualitative and quantitative agreement. Also, for the transitional free shear layer Figure 12 exhibits the spatial development of the three-dimensionality (development of secondary instability).

We carried out other comparison calculations with other shear layer experiments to convince ourselves that our numerical method works properly. So far, we have had only positive experiences and, therefore, we conclude that we are prepared to apply our method now to wake simulations. In summary, together with the numerical methods we have developed and tried previously, we have the following computer codes that can be readily applied to wake investigations:

- a. Two-Dimensional, Temporal (Spatially Periodic)
 - Finite Difference in y , Finite Difference in x
 - Finite Differences in y , Pseudo-Spectral in x
- b. Two-Dimensional, Spatial (Amplification in x)
 - Finite Differences in x and y
- c. Three-Dimensional, Temporal (Periodic in x)
 - Finite Differences in y and x , Pseudo-Spectral in z (Spanwise)
 - Finite Differences in y , Pseudo-Spectral in x and z

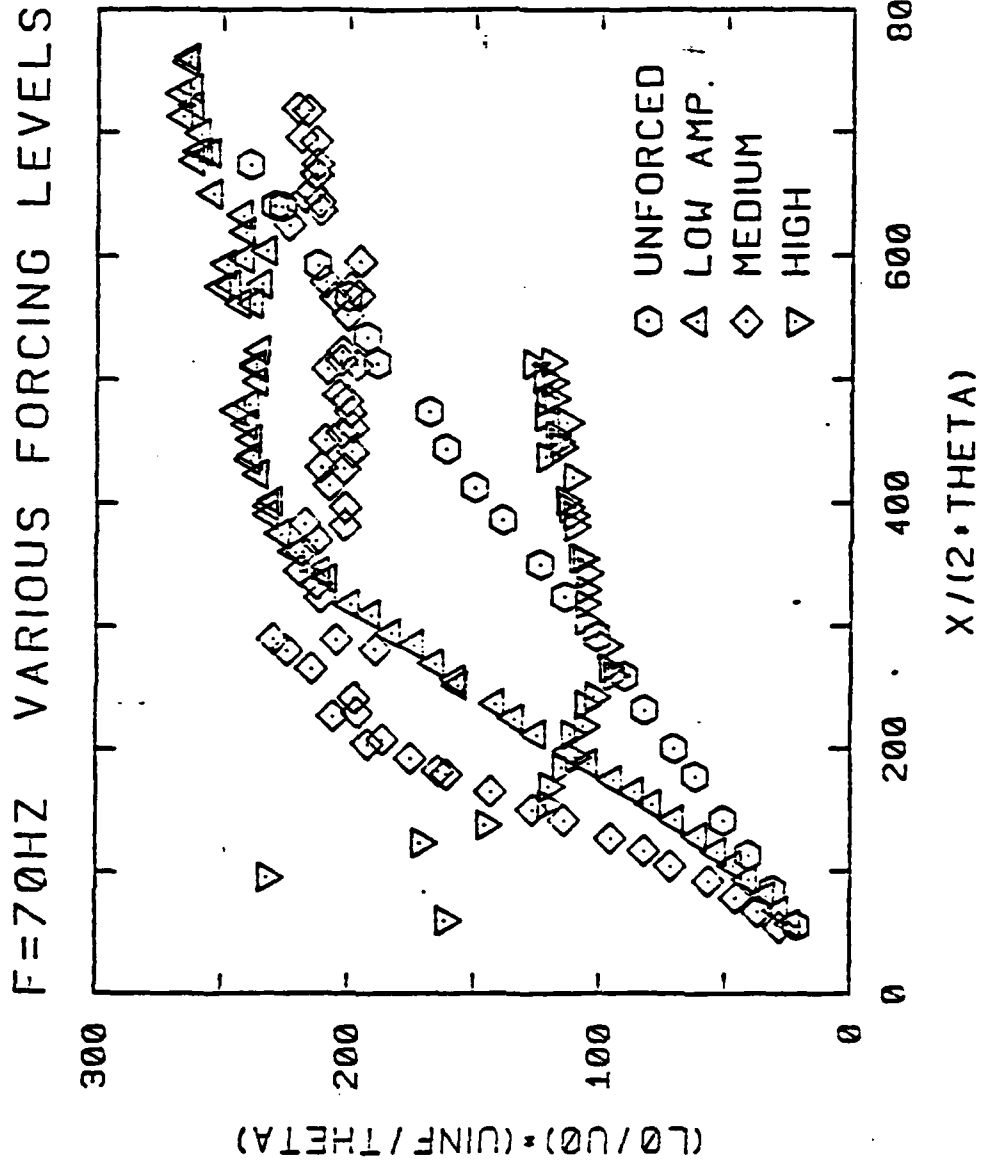


Figure 1. The downstream development of the growth parameter for $f = 70 \text{ hz}$ and various forcing levels.

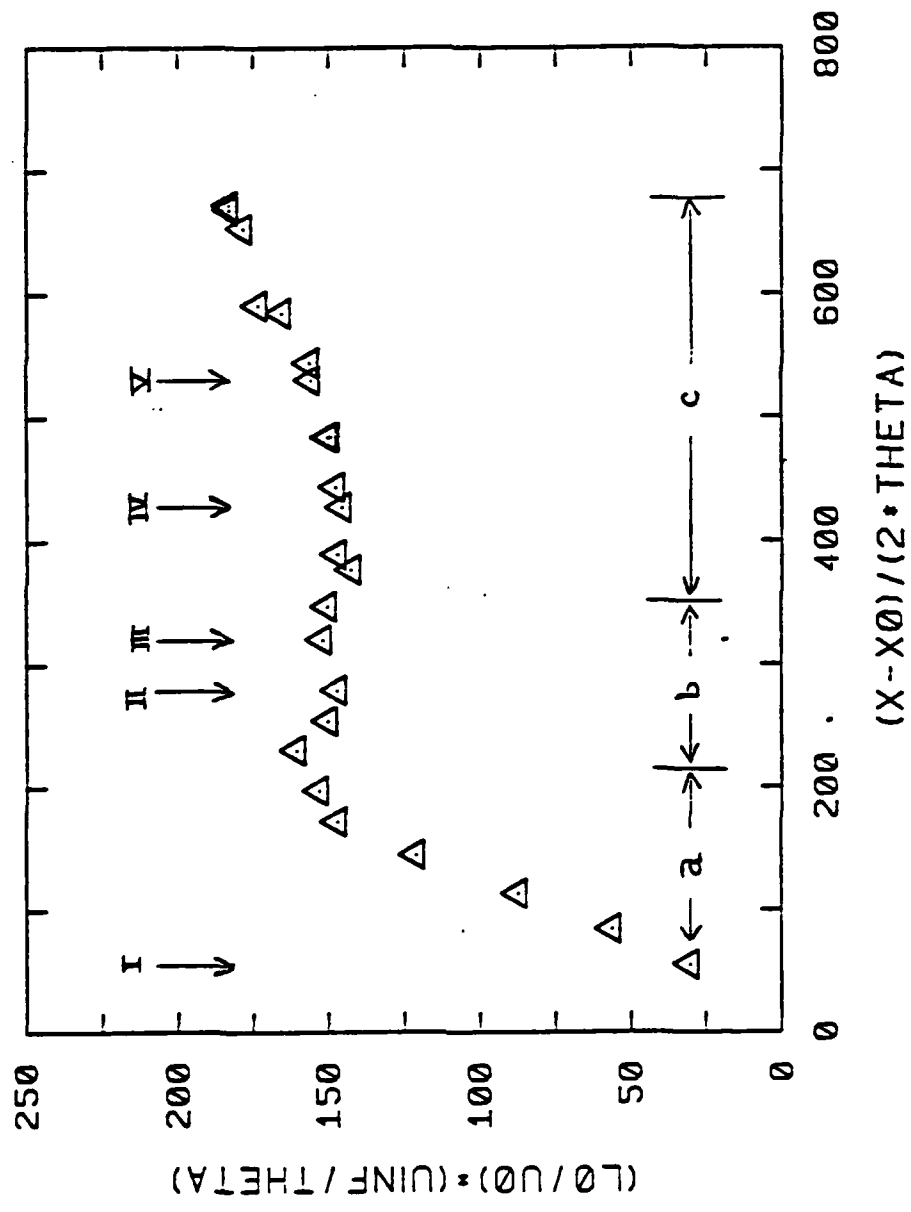


Figure 2. The downstream evolution of the growth parameter for a medium amplitude forcing and $f = 80$ Hz. Downstream regions defined.

NORMALIZED U PROFILES

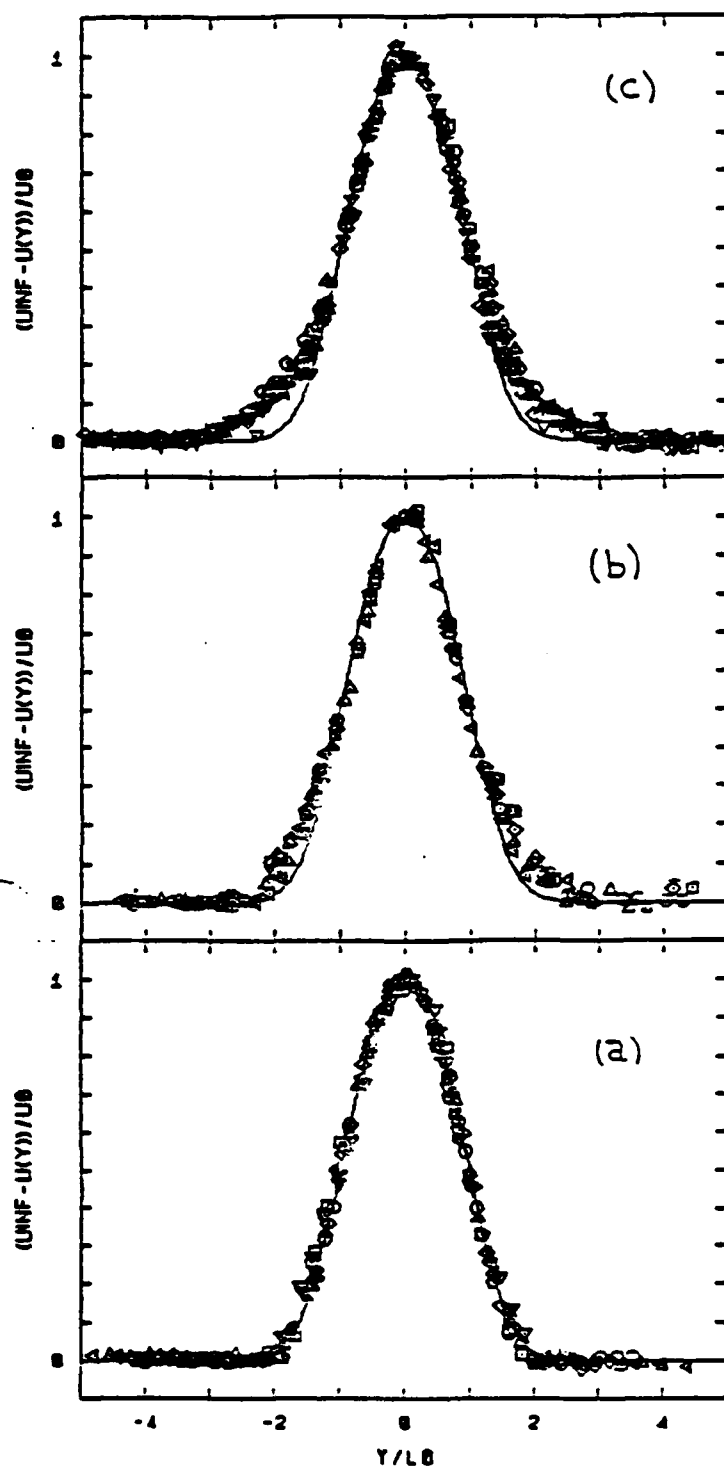


Figure 3. Measured mean velocity profiles in the three defined regions: (a) the amplified region; (b) the neutral region; (c) the damped region.

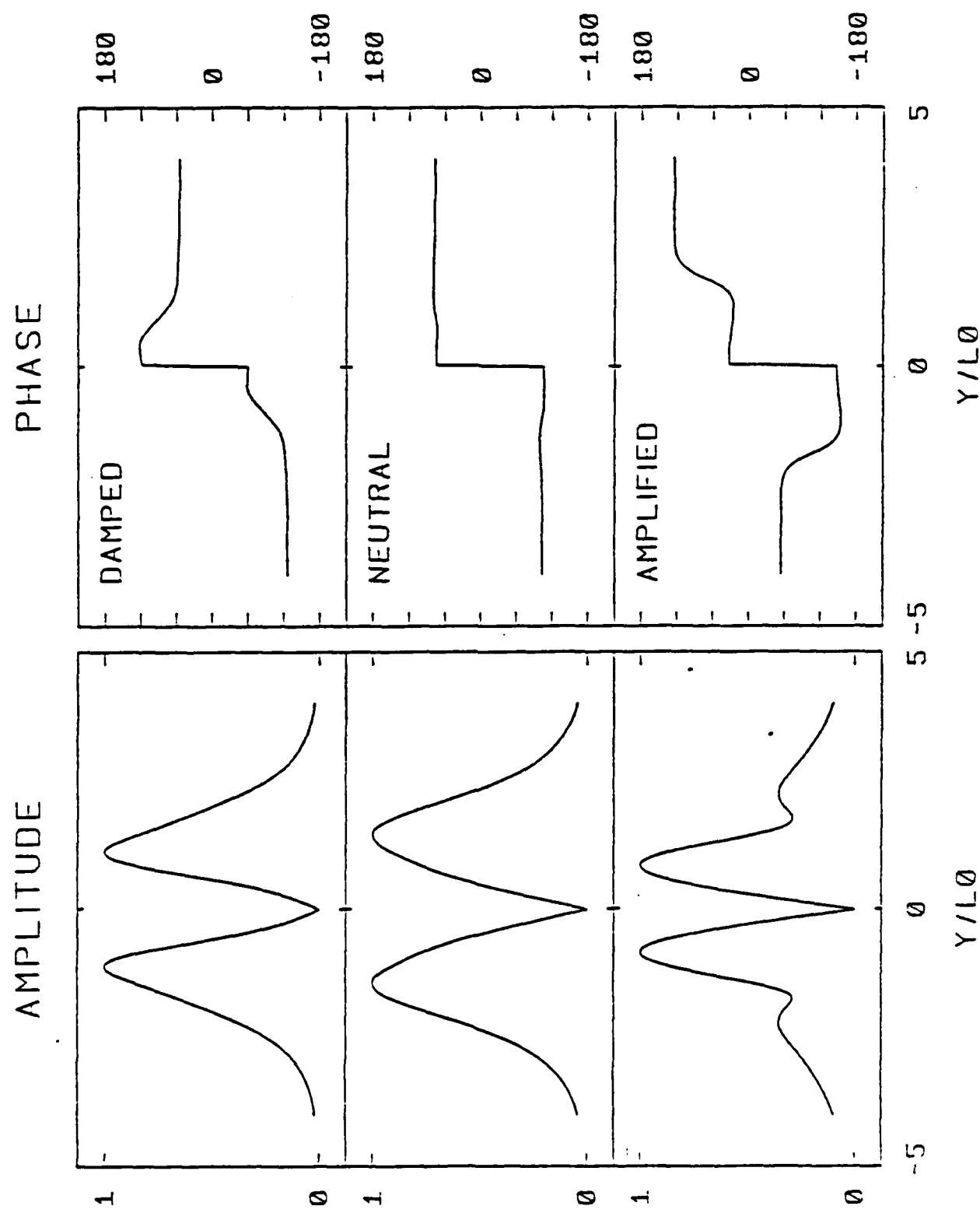


Figure 4. Computed amplitude and phase distributions for u component of disturbance wave typical of amplified, neutral and damped regions from linear stability theory.

COMPUTED REYNOLDS STRESS
FROM LINEAR THEORY

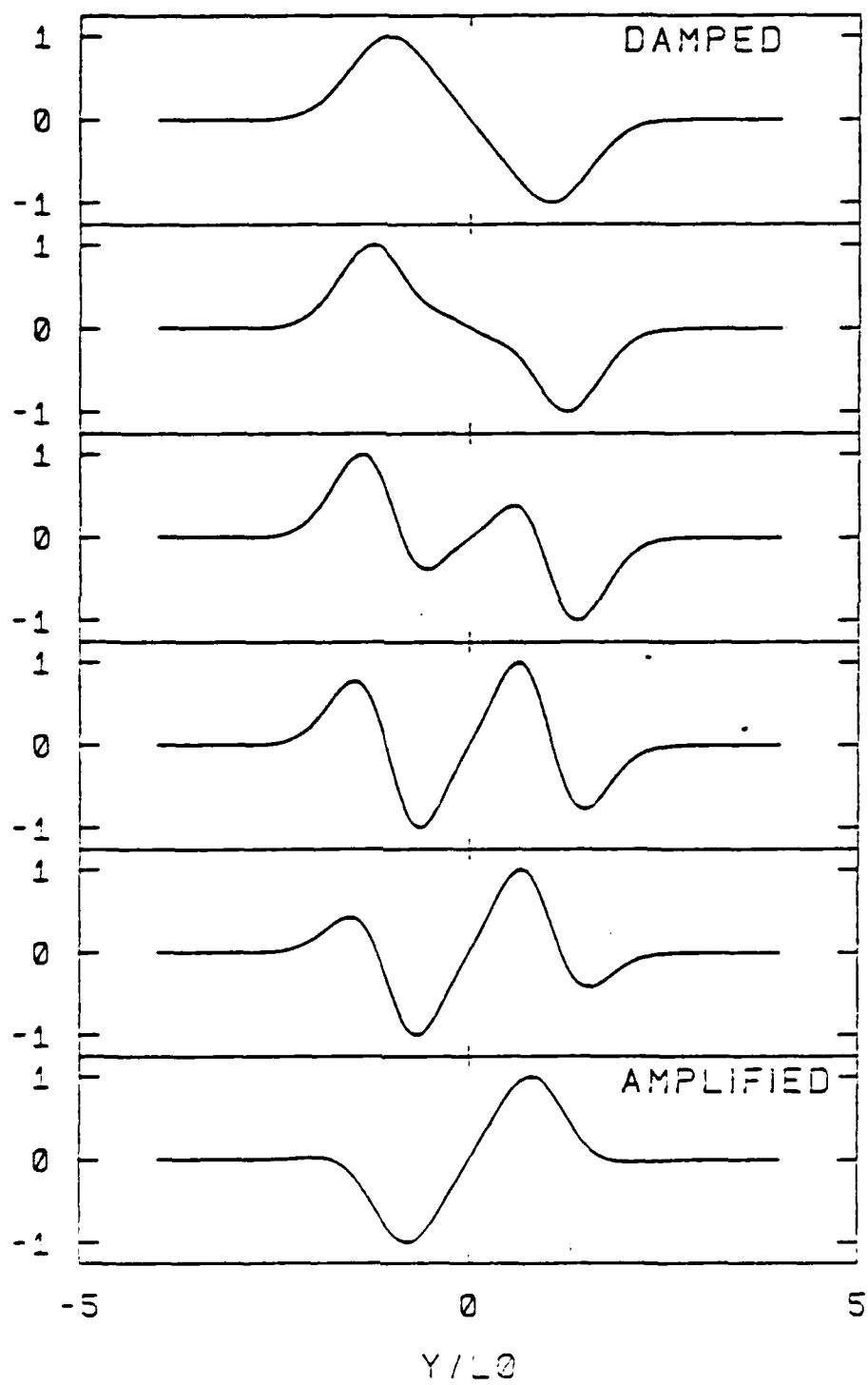


Figure 6. Computed wave induced Reynolds stress distribution for amplified, neutral and damped regions for linear stability theory. Four plots are presented for neutral region.

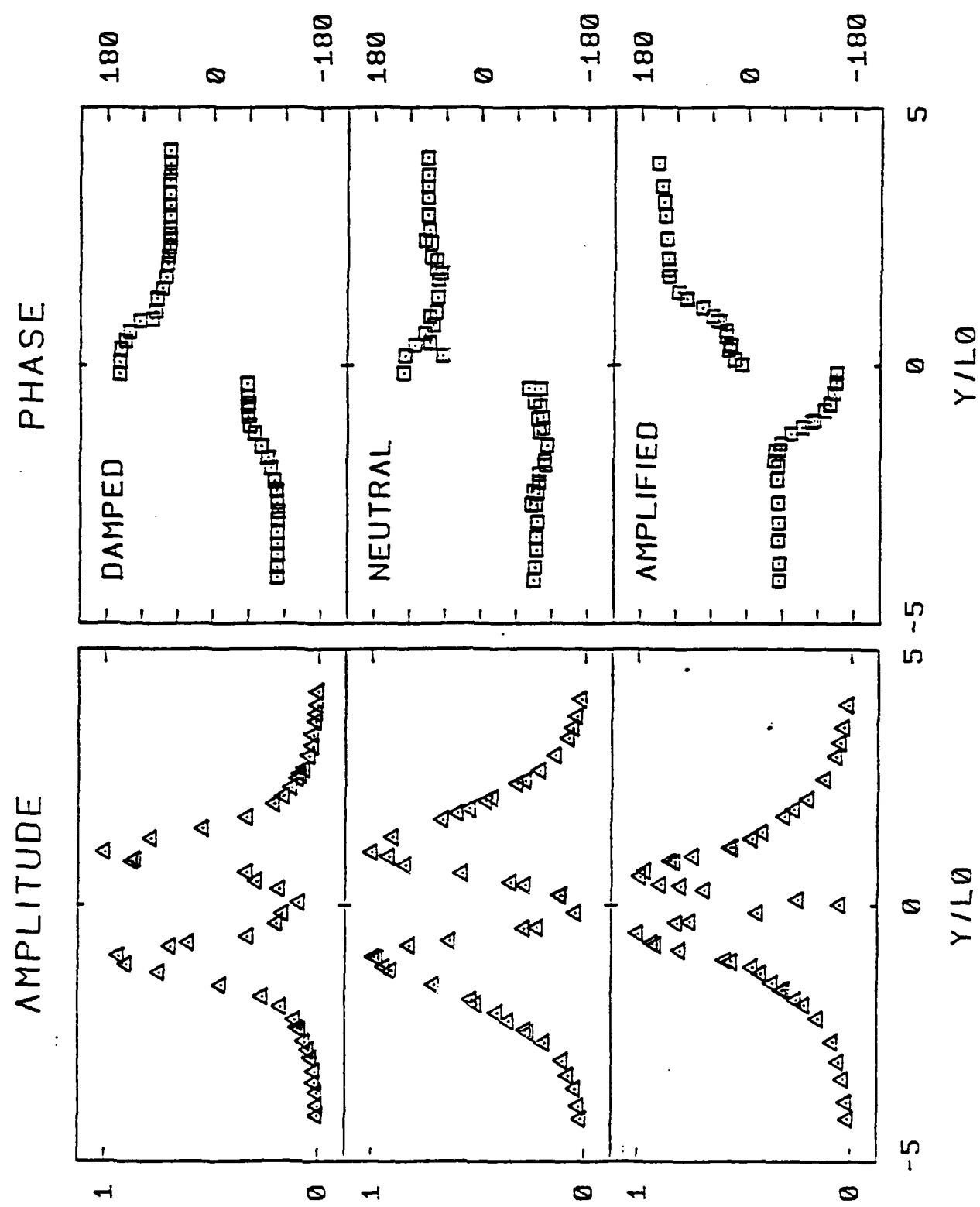


Figure 6. Typical measured amplitude and phase distributions of u component for the three regions.

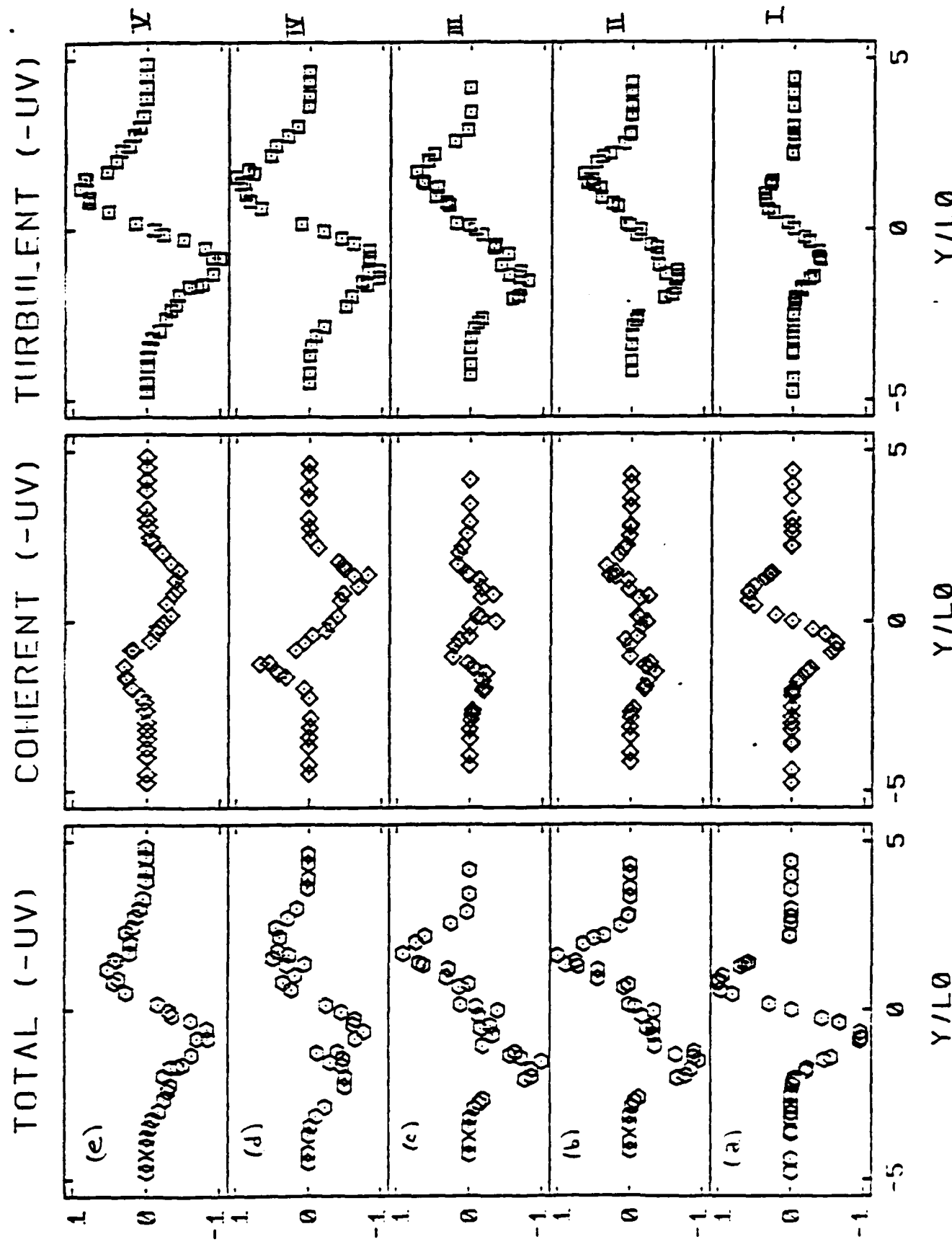


Figure 7. Typical measured distributions of total, wave-induced or coherent, and turbulent Reynolds stresses for the downstream locations identified in Figure 2.

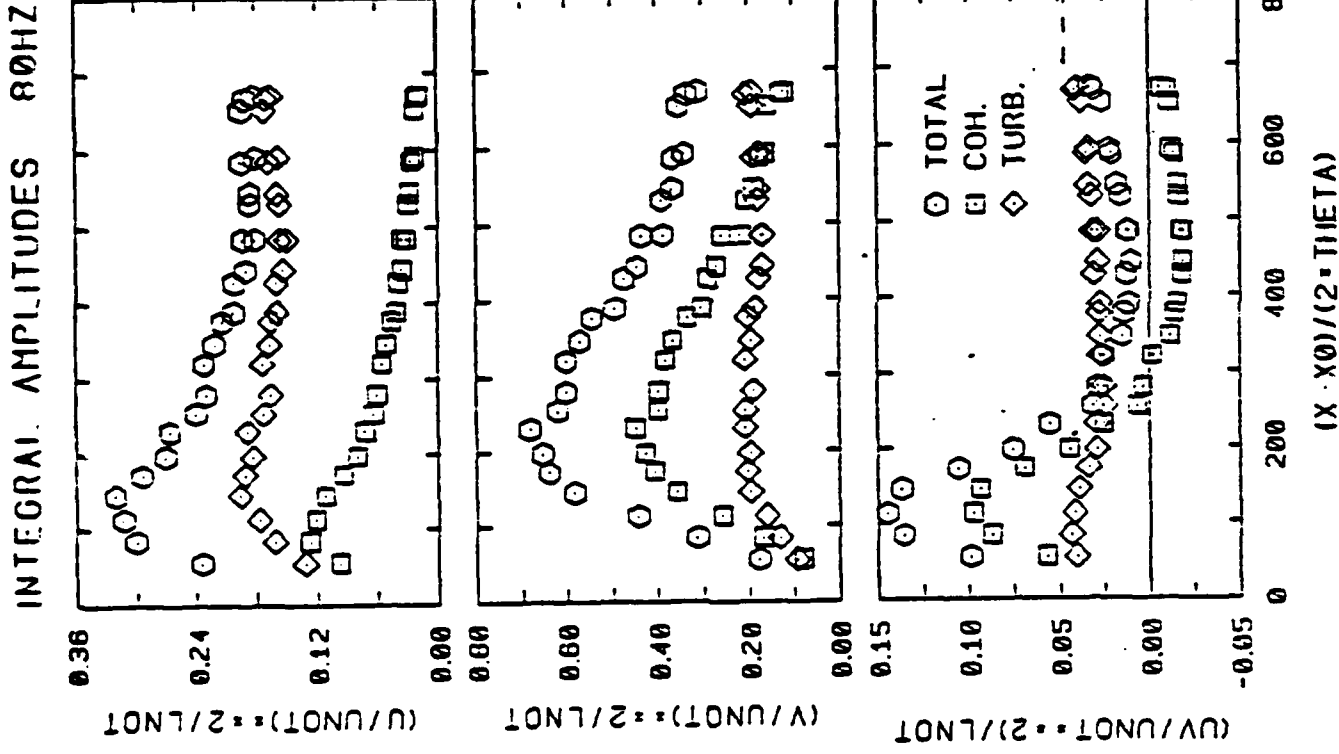


Figure 8.

The downstream development of the integral amplitudes of u_2 , v_2 , and uv in the wave component at the fundamental frequency (coherent). Also shown are the total and turbulent counterparts. x_0 is zero for this case.

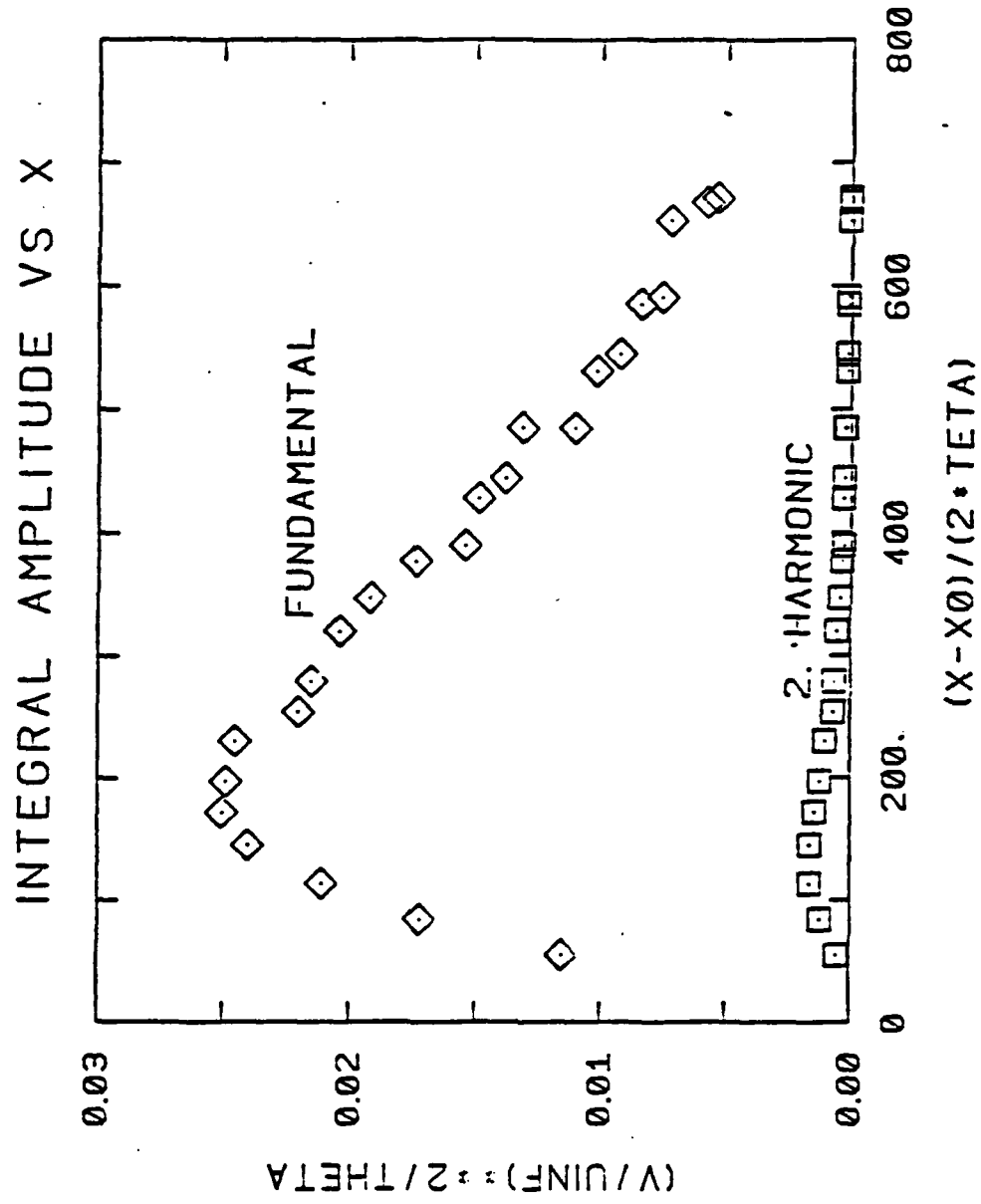


Figure 9. The downstream evolution of the integral amplitude of the fundamental and harmonic for the v-component of the disturbance wave. Data normalized by U_{∞} and Θ .

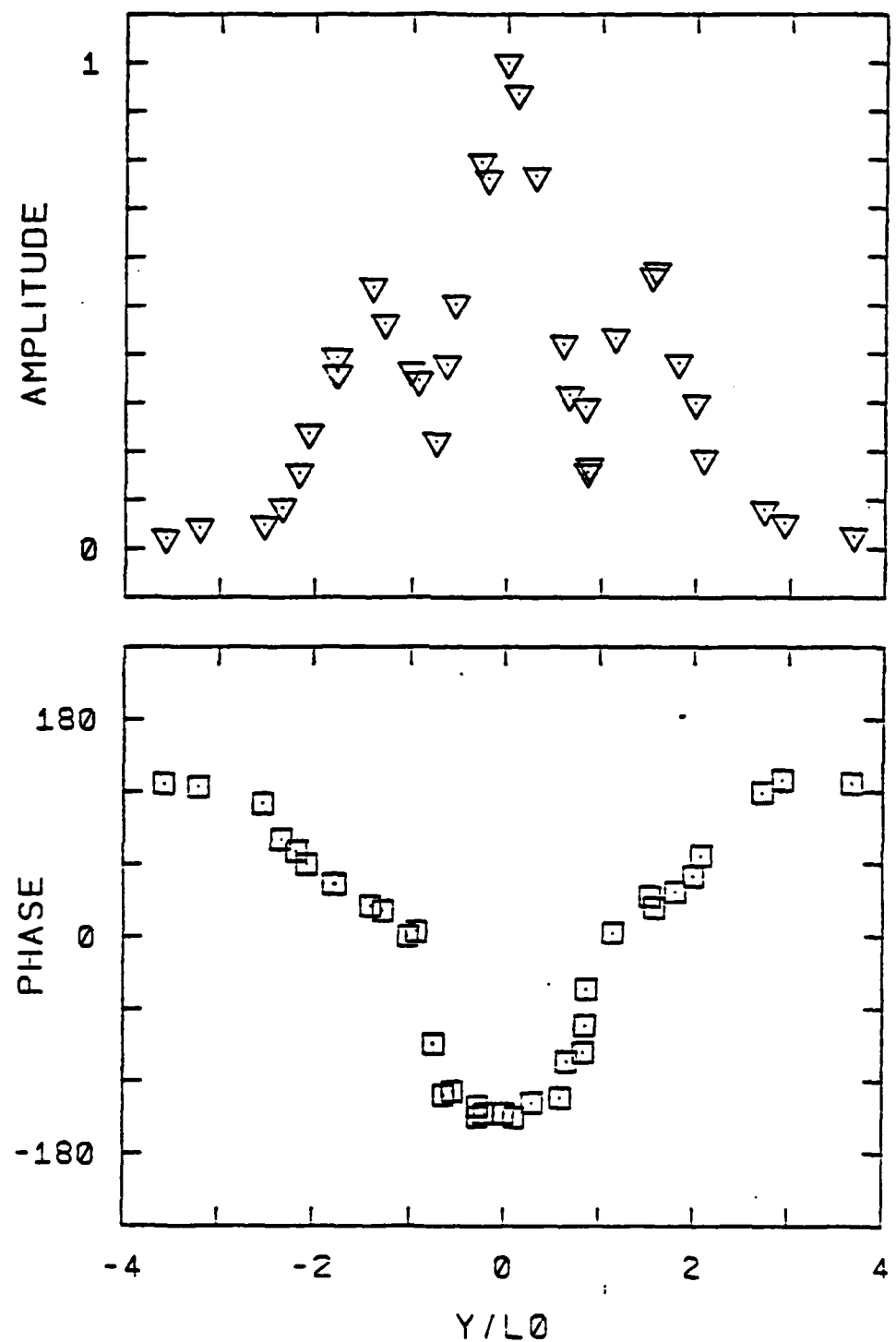


Figure 10. The measured and phase distribution of the harmonic for the u -component at the end of region (a).

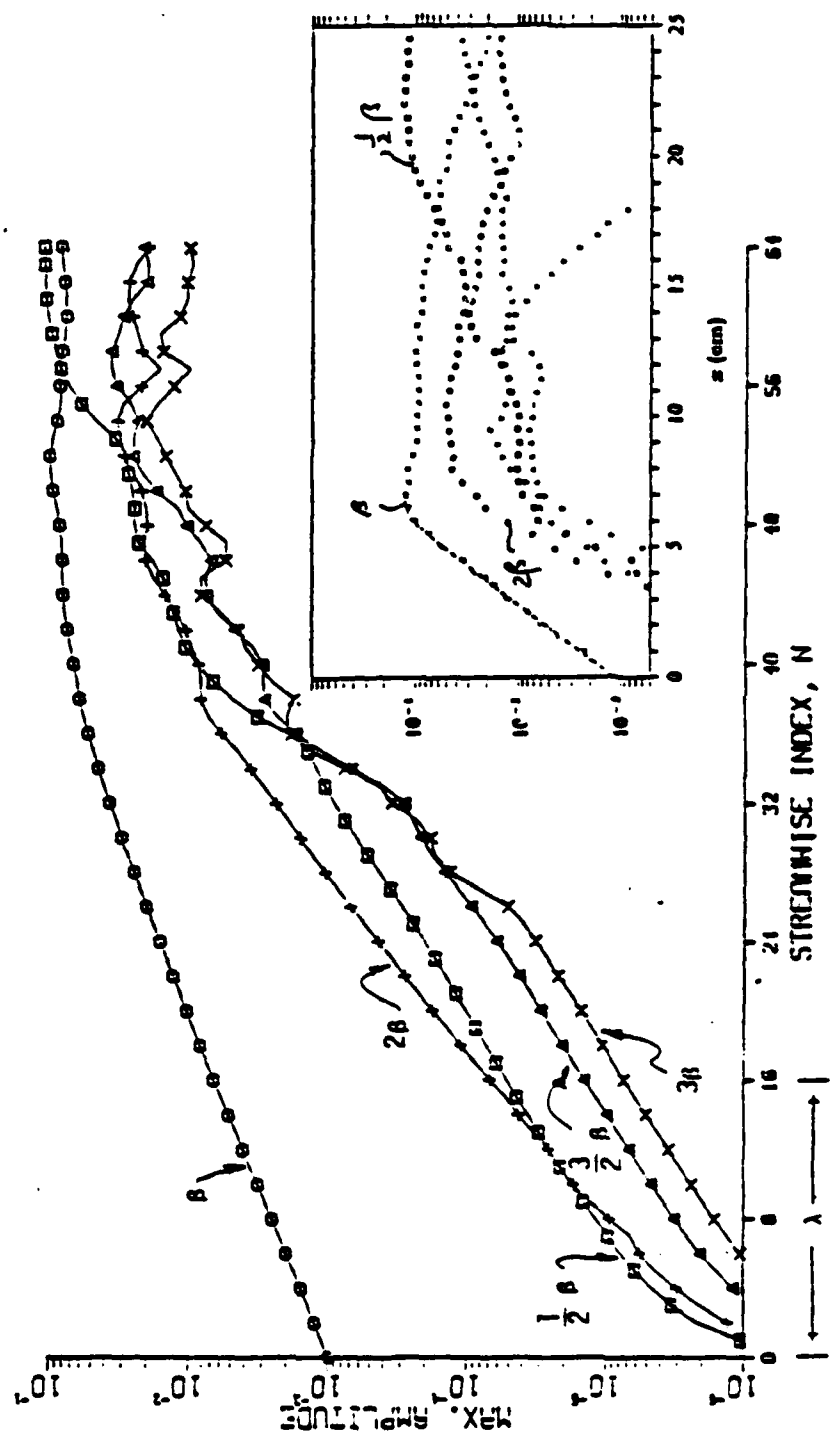


Figure 11. Growth of u_1 -velocity spectra maxima (Inset from Miksad, 1972).
Transitional free shear layer

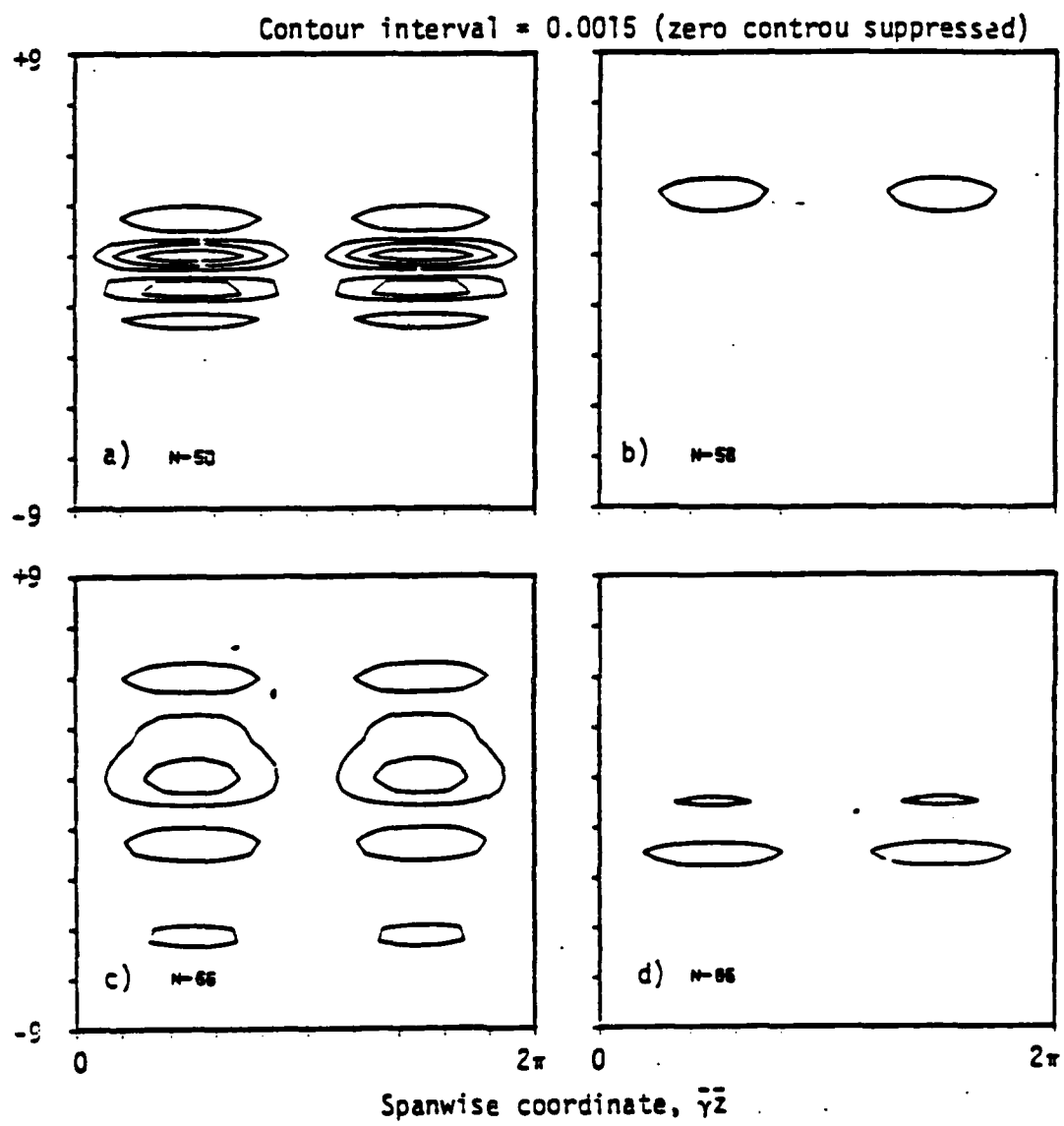


Figure 12. Evolution of streamwise vorticity a) $n=50$, b) $n=58$,
c) $n=66$, d) $n=86$.

$(n=x)/\Delta x$ Transitional free shear layer.

E A N D

5 = 87

D T i C